KEK Preprint 95-23
May 1995
A

Free-Electron Laser Amplifiers in the Microwave Regime - High Power and Bunching -

S. HIRAMATSU

Lecture at the US-CERN-Japan Topical Course on Accelerator Physics & Technology, "Frontiers of Accelerator Technology", Maui, Hawaii, November 3 - 9, 1994.

National Laboratory for High Energy Physics, 1995

KEK Reports are available from:

Technical Information & Library
National Laboratory for High Energy Physics
1-1 Oho, Tsukuba-shi
Ibaraki-ken, 305
JAPAN

Phone: 0298-64-5136
Telex: 3652-534 (Domestic)
(0)3652-534 (International)
Fax: 0298-64-4604
Cable: KEK OHO
E-mail: Library@kekvax.kek.jp (Internet Address)

Free-Electron Laser Amplifiers in the Microwave Regime - High Power and Bunching -

S. HIRAMATSU

Natinal Laboratory for High Energy Physics, 1-1 Oho, Tsukuba, Ibaraki, 305, Japan

E-mail: hiramatu@kekvax.kek.jp

ABSTRACT

The basic theory of free-electron lasers in the microwave regime driven by a high current and low energy electron beam is described taking account of the space charge effect, energy spread and emittance of the electron beam. The experimental studies of high power microwave FEL amplifiers at LLNL, KEK and CESTA are reviewed.

1. Introduction

A free-electron laser (FEL) is a tunable amplifier of coherent radiation. A relativistic electron beam interacts with the traveling electromagnetic wave in the ulternating static magnetic field produced by a wiggler and the energy of electrons is transformed into electromagnetic wave. An FEL can produce high-power coherent radiation in a wavelength range extending from cm to VUV region. After the first investigation on an FEL in the microwave region (λ=5mm), so called Ubitron, by R.Phillips in 1957[1], the first generation of the coherent radiation in the short wavelength region (λ=10.6μm and 3.4μm) from the FEL was demonstrated at Stanford University by J.Madey et al. in 1975[2,3]. After these pioneering experiments, numerous FEL programs have been established in the wide range of wavelength. As for the FEL in the microwave regime, a high-power FEL with the amplified radiation power of more than hundred MW is considered as one of the candidates of rf-source for plasma heating in the fusion field and for the linear collider with high accelerating gradient. An excellent experimental program of the microwave FEL was established at LLNL with an FEL amplifier producing the 1GW radiation at 35GHz[4,5,6]. Futhermore, A.M.Sessler proposed the concept of a two-beam accelerator with high-power microwave FELs (TBA/FEL) driven by induction linacs as one of the promissing concepts for the future linear collider[7,8]. In this paper, however, we have no space to discuss the TBA/FEL and we will confine our interests to the high-power microwave FELs. Basic physics of FELs is described and the typical experiments are reviewed in the following.

For the net exchange of energy between electrons and electromagnetic wave in the wiggler field, it is required to satisfy the synchronism condition of $c\beta_z \approx \omega/(k_w + k)$ which has the familiar expression of $\lambda \approx \lambda_w/2\gamma_z^2$ in the approximation of $\gamma >> 1$, where $c\beta_z$ is the axial drift velocity of electrons in the wiggler field, λ is the wavelength of the electromagnetic field, λ_w is a period length of the wiggler and $\gamma_z = 1/\sqrt{1-\beta_z^2}$. Since the exponential gain and the saturation power of an FEL are proportional to $I^{1/3}$ in the Compton regime ($I^{1/4}$ and $I^{1/2}$, respectively, in the Raman regime)[9], a high-power FEL in the microwave region are driven by a low energy and high current electron beam as shown in Fig. 1. Where the Compton FEL means that the gain is not affected by the longitudinal space charge effect in the electron beam and I is the electron beam current. In the Raman FEL, the gain is dominated by the space charge effect. If we have strong space charge effect, the peak position of the FEL gain shifts toward low B_w side. The performance of an FEL is also strongly affected by the energy spread and the emittance of the electron beam.

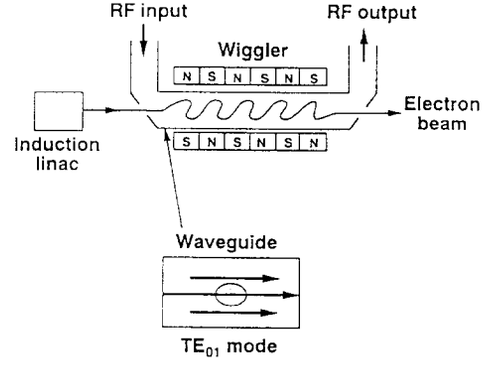

Fig. 1 The high gain free-electron laser in the microwave regime.

There is noteworthy difference between the high gain FEL and the low gain FEL which is familiar in the visible light or UV region. The gain of a low gain FEL is zero at resonance and the maximum gain is obtained at the energy slightly higher than the resonance energy. On the other hand, the maximum gain is obtained at the resonance energy in the high gain FEL. These properties are described by a cubic dispersion relation for FELs.[6,9,10]

2. Basic Theory

2.1. KMR Equations

Basic FEL equations which describe the electron motion and electromagnetic field evolution in the wiggler field are derived from the single particle Hamiltonian of the electron and the Maxwell equation. Considering the planar wiggler and the single waveguide mode of the electromagnetic wave, the Hamiltonian and the Maxwell equation are given by

$$H=\left[m^2c^4+c^2\left(\boldsymbol{P}+e\boldsymbol{A}_w+e\boldsymbol{A}_s\right)^2\right]^{1/2}+e\Phi, \tag{1}$$

$$\left(\nabla^2-\frac{1}{c^2}\frac{\partial^2}{\partial t^2}\right)\boldsymbol{A}_s=-\mu_0\boldsymbol{J}_\perp, \tag{2}$$

where $\boldsymbol{P}$ is the canonical momentum, $\boldsymbol{J}_\perp$ is the transverse component of the current density, $\boldsymbol{A}_w$ and $\boldsymbol{A}_s$ are the vector potentials of the wiggler field and the electromagnetic field of the TE_{01} mode in the waveguide with the cross section of $a\times b$, respectively,

$$\boldsymbol{A}_w=A_w\cosh(k_wy)\sin(k_wz)\cdot\boldsymbol{e}_x, \tag{3}$$

$$\boldsymbol{A}_s=A_s\cos\left(\frac{\pi}{b}y\right)\sin(kz-\omega t+\phi)\cdot\boldsymbol{e}_x, \tag{4}$$

and the wave number k of the electromagnetic field is $k=\sqrt{(\omega/c)^2-(\pi/b)^2}$. From these equations the basic one-dimensional FEL equations, so called KMR equations, are derived[12];

$$\frac{d\gamma}{dz}=-\frac{\omega/c}{2\gamma\beta_z}a_wf_Ba_s\sin\psi-\frac{e}{mc^2\beta_z}\boldsymbol{\beta}\cdot\boldsymbol{E}_{sc} \tag{5}$$

$$\frac{d\psi}{dz}=k_w+k-\frac{\omega/c}{\beta_z}\left\{1-\frac{a_wf_B}{2\gamma^2{\beta_z}^2}a_s\cos\psi\right\}+\frac{d\phi}{dz}, \tag{6}$$

$$\frac{da_s}{dz}=\frac{e\mu_0}{2mck}\frac{2I}{ab}a_wf_B\left\langle\frac{\sin\psi}{\gamma\beta_z}\right\rangle, \tag{7}$$

$$\frac{d\phi}{dz}=\frac{e\mu_0}{2mck}\frac{2I}{ab}\frac{1}{a_s}\left[a_wf_B\left\langle\frac{\cos\psi}{\gamma\beta_z}\right\rangle-a_s\left\langle\frac{1}{\gamma\beta_z}\right\rangle\right], \tag{8}$$

where $\boldsymbol{E}_{sc}=-\boldsymbol{grad}\Phi$ is the space charge field, $a_w=eA_w/mc=eB_w/mck_w$ and $a_s=eA_s/mc$ are the normalized vector potentials, $\psi=(k_w+k)z-\omega t+\phi$ is the ponderomotive phase, $f_B=J_0(\xi)-J_1(\xi)$ represents the effective coupling between the wiggle motion of the electron and the electromagnetic wave in the planar wiggler field, $\xi=(\omega/c)a_w{}^2/8\gamma^2{\beta_z}^2$, $2/ab$ is the effective mode area of the TE_{01} waveguide mode and $\langle\cdots\rangle$ means the average in a period of ψ. The axial drift velocity β_z averaged in a wiggler period of the electron is given by

$$\beta_z=\left[1-\frac{1+\left(a_w^2/2\right)\cosh^2(k_w\bar{y})}{\gamma^2}-{\beta_\perp}^2\right]^{1/2}, \tag{9}$$

where $\beta_\perp=\hat{\beta}_z\sqrt{\bar{x}'^2+\bar{y}'^2}$ is the transverse velocity component of the betatron oscillation due to the wiggler intrinsic focusing[11] and the additional focusing. In the following the additional focusing is assumed to be weak compared to the wiggler intrinsic focusing and we will take account of the intrinsic focusing alone;

$$\bar{x}'\approx 0, \tag{10}$$

$$\bar{y}'=k_\beta y_\beta\sin\left(k_\beta z+\phi_\beta\right), \tag{11}$$

$$\bar{y}=y_\beta\cos\left(k_\beta z+\phi_\beta\right), \tag{12}$$

$$k_\beta=\frac{a_wk_w}{\sqrt{2}\gamma}. \tag{13}$$

It is easily seen that KMR equations satisfy the conservation low of the total energy of electrons and the electromagnetic field,

$$\frac{d}{dz}\left(P_b+P_{rf}\right)=0, \tag{14}$$

where $P_b = \left(mc^2 I/e\right)\langle \gamma - 1 \rangle$ and $P_{rf} = \left(m^2 c^2 \omega \alpha b / 4\mu_0 e^2\right) a_s{}^2$ are the energy flows of the electron beam and the electromagnetic field. For a net energy exchange between electrons and the electromagnetic wave, the ponderomotive phase ψ must be stationaly. Because the effect of the electromagnetic field to the electron orbit is small, the synchronism condition or the resonance condition is expressed by

$$\beta_z = \frac{\omega / c}{k_w + k} \ . \tag{15}$$

The axial velocity spread caused by the energy spread and the beam emittance degrades the FEL performance. For the case of $k_w{}^2 y^2 << 1$, the initial axial drift velocity is given by

$$\beta_z \equiv \hat{\beta}_z + \frac{1 + a_w^2/2}{\hat{\beta}_z \gamma_0^2} \frac{\Delta\gamma}{\gamma_0} - \frac{a_w^2 k_w^2}{4\hat{\beta}_z \gamma_0^2} y_\beta^2 , \tag{16}$$

where γ_0 is the average of electron's γ, $\gamma_0 + \Delta\gamma$ is the initial electron energy, and $\hat{\beta}_z$ is the axial drift velocity for $\gamma = \gamma_0$ and $y_\beta = 0$;

$$\hat{\beta}_z = \left(1 - \frac{1 + a_w^2/2}{\gamma_0{}^2}\right)^{1/2} . \tag{17}$$

Assuming the uniform distribution of electrons in the elliptic betatron phase space of $(\bar{y}, \bar{y}')$, average of $y_\beta{}^2$ is given by $\left\langle y_\beta{}^2 \right\rangle = y_b{}^2/2$ for the vertical half beam size of y_b. The vertical betatron oscillation shifts the axial velocity and causes the axial velocity spread. These effects are expressed by the equivalent energy shift $(\Delta\gamma/\gamma_0)_{shift}$ of the electron beam and the effective energy spread $(\Delta\gamma/\gamma_0)_{eff}$;

$$\left(\frac{\Delta\gamma}{\gamma_0}\right)_{shift} = -\frac{a_w^2 k_w^2}{8\left(1 + a_w^2/2\right)} y_b^2 , \tag{18}$$

$$\left(\frac{\Delta\gamma}{\gamma_0}\right)_{eff} \approx \left[\left(\frac{\Delta\gamma}{\gamma_0}\right)^2 + \left\{\frac{a_w^2 k_w^2}{8\left(1 + a_w^2/2\right)} y_b^2\right\}^2\right]^{1/2} . \tag{19}$$

2.2. *rf-Bucket (Ponderomotive Well)*

As well as rf-acceleration in a synchrotron, electrons are trapped in the rf-bucket (or ponderomotive well). The resonance γ and ψ are defined by

$$\beta_{zr} \equiv \left(1 - \frac{1 + a_w^2/2}{\gamma_r^2}\right)^{1/2} = \frac{\omega / c}{k_w + k} , \tag{20}$$

$$\frac{d\gamma_r}{dz} = -\frac{\omega / c}{2\gamma_r \beta_{zr}} f_B a_w a_s \sin\psi_r . \tag{21}$$

The equations of the $\Delta\gamma = \gamma - \gamma_r$ and ψ are derived from the Hamiltonian[12,13] of

$$\mathcal{H}(\psi, \Delta\gamma; z) = \frac{(\omega/c)\left(1 - \beta_{zr}{}^2\right)}{2\gamma_r \beta_{zr}^3} (\Delta\gamma)^2 - \frac{\omega/c}{2\gamma_r \beta_{zr}} f_B a_w a_s \left(\cos\psi + \psi \sin\psi_r\right), \tag{22}$$

and the electron trajectory in the $(\psi, \Delta\gamma)$ phase space is given by $\mathcal{H}$=costant. In Eq.(22) $a_w a_s / \gamma^2 << 1$ is assumed for the simplicity.

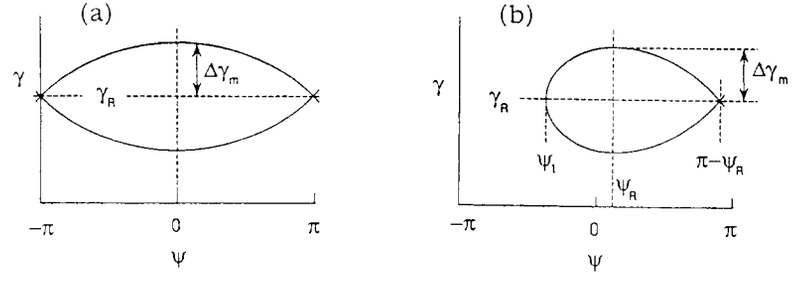

Fig. 2 The rf-bucket in the FEL interaction. The stationary rf-bucket (a) for $da_w/dz = 0$ $(\sin\psi_r = 0)$ and the decelerating rf-bucket (b) for $da_w/dz < 0$ $(\sin\psi_r > 0)$.

The separatrix which represents the boundary between bound and unbound orbits in the phase space is given by

$$(\Delta\gamma)^2 = \frac{\beta_z^2 f_B a_w a_s}{1-\beta_z^2}\left\{\cos\psi + \cos\psi_r + (\psi+\psi_r-\pi)\sin\psi_r\right\}. \tag{23}$$

Assuming the constant a_s, electrons are trapped in the constant rf-bucket for $da_w/dz = 0$ (Fig. 2(a)) and in the decelerating rf-bucket for $da_w/dz < 0$ (Fig. 2(b)) because of $\sin\psi_r \propto -(da_w/dz)/a_w a_s$. Electrons trapped in the ponderomotive well are bunched with the spatial period of the ponderomotive well, $2\pi/(k_w+k)$, as shown schematically in Fig. 3. It is useful to define the bunching parameter[14,15] as

$$B = \left|\left\langle e^{i(\psi-\phi)}\right\rangle\right|, \tag{24}$$

which is unity for the delta-function like bunch.

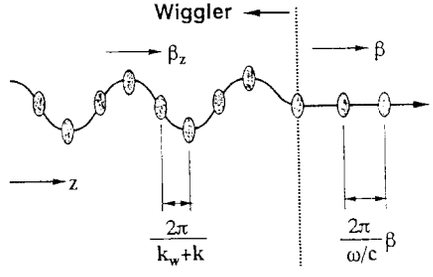

Fig. 3 Electron bunches in the wiggler.

In Fig. 4 is shown the simulation result based on Eqs.(5)-(8) without the space charge effect for the kinetic energy of electrons of T=3MeV, the energy spread of $\Delta T/T = \pm 1\%$, the beam current of I_b=850A and the rf frequency of f=34.6GHz. The shift and spread of the axial velocity by the betatron oscillation is not taken into account in the calculation. The solid line shows evolution of the rf-power as a function of the interaction length in the constant wiggler.

(a)

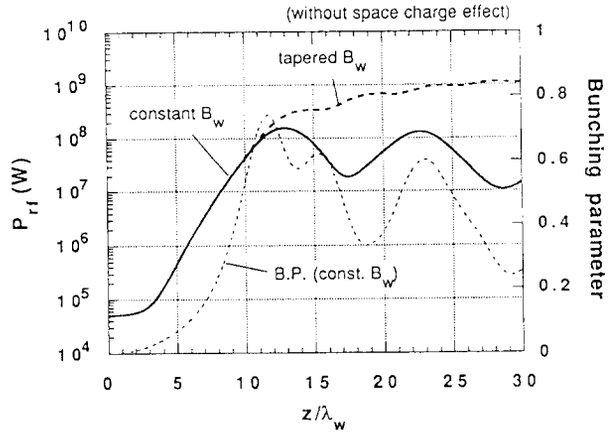

(b)

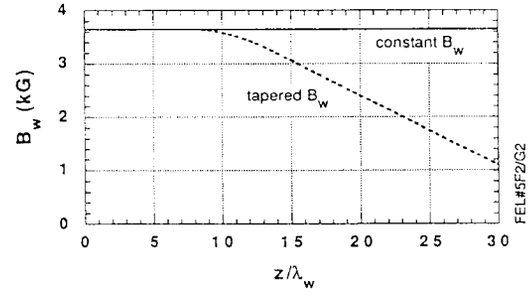

Fig. 4 The amplified rf-power and the bunching parameter in the FEL calculated by the 1D simulation code with a single waveguide mode (TE_{01}-mode). (a) The solid curve and the dashed curve are the rf-power in the constant wiggler and in the tapered wiggler, respectively, and the dotted curve is the bunching parameter in the constant wiggler. The wiggler field strength is shown in (b) as a function of z/λ_w.

As is shown in Fig. 5 electrons rotate downward in the rf-bucket, the average energy of electrons reaches its minimum value at the interaction length of z/λ_w=13 and the amplified rf power saturates. After saturation the rf-power oscillates according to the synchrotron oscillation of electrons in the rf bucket. Tapering the wiggler field as shown in Fig. 4(b) to maintain the synchronism condition stationally beyond saturation, a considerable fraction

of electrons are trapped in the decelerating rf-bucket (Fig. 5(d)) and the amplified rf power increases monotonically beyond saturation as shown in Fig. 4(a) by the dashed curve. In this example we can expect the saturation power of 150MW for the constant wiggler and about 1GW amplified power for the tapered wiggler of 3m long. As for the bunching performance, the maximum bunching parameter of B=0.74 is expected in the vicinity of the saturation point and the electron current in a period of ψ is depicted in Fig. 6. This suggests the good performance of an FEL for the buncher in the high frequency region. The FEL buncher for the CLIC driving beam was proposed by S.S.Yu et al.[14] and experimental study is going on at CESTA.[16]

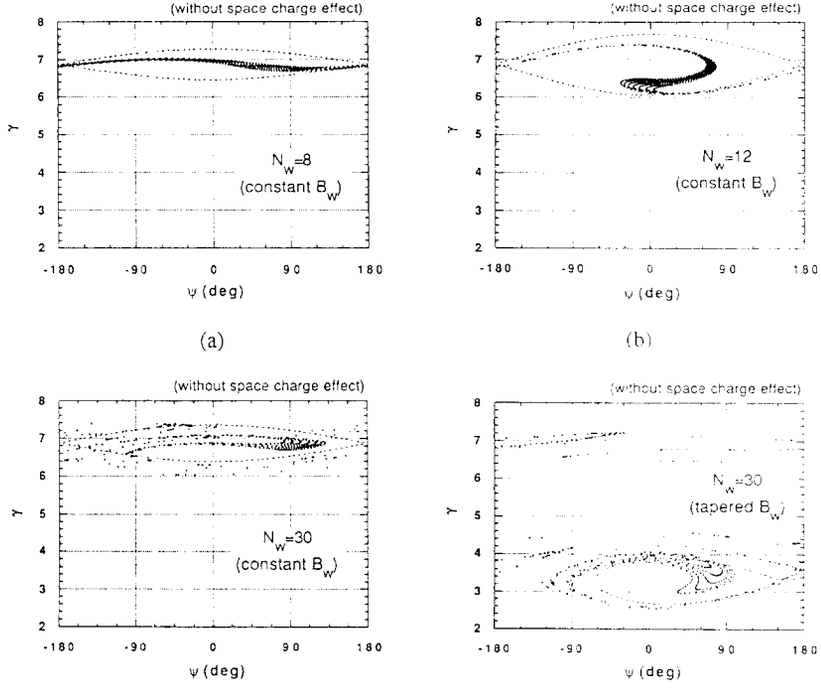

Fig. 5 Electron distribution in the longitudinal phase space. Distributions in the constant wiggler (a)-(c) and in the tapered wiggler (d).

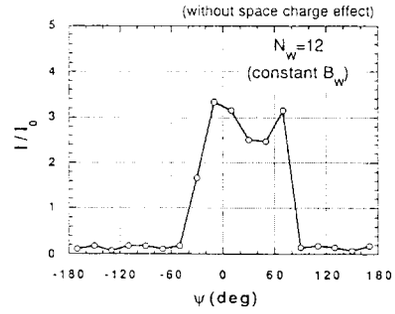

Fig. 6 Electron current in a wavelength.

Another application of the bunching component of the electron current is the "after-burner[17,18]" which is the resonant cavity to extract the rf-power from the electron beam passed through the FEL interaction region. It is expected to increase the total extraction efficiency using the after-burner.

2.3. Longitudinal Space Charge Effect

In the high gain FEL driven by a high current electron beam, the gain of the FEL is strongly affected by the longitudinal space charge effect. The energy change of the electron by the space charge field is expressed by

$$\frac{d\gamma}{dz} = -\frac{e}{mc^2}\frac{\beta}{\beta_z}E_s, \tag{25}$$

where s is the length along the beam center orbit, $\boldsymbol{e}_s = \boldsymbol{\beta}_0/\beta_0$ is the unit vector in the instantaneous direction of the wiggle motion, $c\beta_0$ is the electron velocity at the beam center and $E_s = \boldsymbol{e}_s \cdot \boldsymbol{E}_{sc}$ is the s-component of the space charge field. The coordinate system is shown in Fig. 7. The effective longitudinal space charge field is obtained by expanding the beam charge density ρ and the space charge field E_s in the siries of $exp(in\theta)$;

$$\rho = \sum_{n=-\infty}^{\infty}\rho_n e^{in\theta}, \tag{26}$$

$$E_s = \sum_{n=-\infty}^{\infty} \varepsilon_n e^{in\theta}, \tag{27}$$

and solving the Maxwell equation;

$$\left(\left[\nabla^2 - \frac{1}{c^2}\frac{\partial^2}{\partial t^2} \right] E_{sc} \right)_s = \frac{1}{\varepsilon_0}(grad\rho)_s + \mu_0 \frac{\partial J_s}{\partial t}, \tag{28}$$

with an appropriate manner where $\theta = (k_w + k)z - \omega t$.

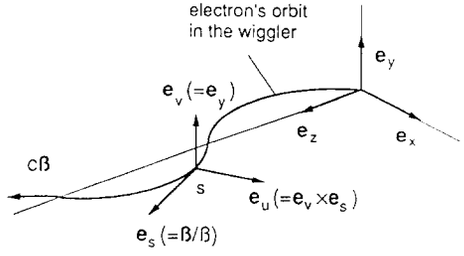

Fig. 7 The coordinate system for calculating the longitudinal space charge field.

Following to E.T.Scharlemann et al.[22] the modified Bessel equation for ε_n is obtained for the round beam by substituting Eqs.(26) and (27) into Eq.(28) and averaging in one wiggler period (see Appendix A). For the uniform charge distribution in the beam cross section, ε_n is given by

$$\varepsilon_n = i\frac{4mc^2(I/I_A)}{ne(k_w + k)r_b^2}\frac{\hat{\beta}_z}{\beta} f_{2D}\left\langle e^{-in\theta}\right\rangle, \tag{29}$$

where r_b is the beam radius, $I_A = 4\pi mc^3\varepsilon_0/e \cong 17kA$ is the Alfven current.

$$f_{2D} \cong 1 - \frac{|n|(k_w + k)}{\gamma} r_b K_1\left\{\frac{|n|(k_w + k)}{\gamma} r_b\right\} \tag{30}$$

is the space charge reduction factor due to the finite beam size and $K_1(x)$ is the modified Bessel function. For the short wavelength FEL such as the visible light or IR region FEL,

f_{2D} is very close to unity, however, for the microwave FEL in the cm-wavelength region this factor is considerably smaller than unity. Recently we recalculated f_{2D} with more precice approximation and different γ dependence has been obtained as described in Appendix A (Eq.(A13)). At present it is not obvious which representation of f_{2D} is correct, and we will take the reduction factor given by Eq.(30) in the following discussion.

Taking the lowest mode ($n = \pm 1$) of the space charge field and averaging in a wiggler period λ_w, the equation of γ (Eq.(5)) is rewritten as

$$\frac{d\gamma}{dz} = -\frac{\omega/c}{2\gamma\beta_z} f_B a_w a_s \sin\psi - \hat{\varepsilon}_s\{\cos\theta\langle\sin\theta\rangle - \sin\theta\langle\cos\theta\rangle\}, \tag{31}$$

where

$$\hat{\varepsilon}_s = \frac{8(I/I_A)}{(k_w + k)r_b^2} J_0(\xi) f_{2D}. \tag{32}$$

The 1D simulation results with and without the space charge effect in a constant wiggler are shown in Fig. 8.

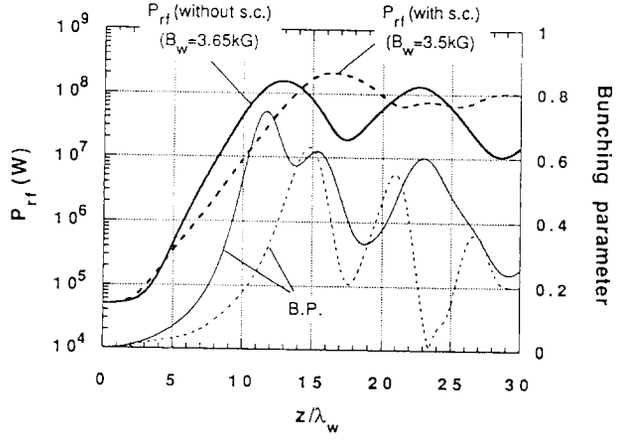

Fig. 8 The 1D simulation results without the space charge effect (solid line) and with the space charge effect (dashed line). The FEL parameters for the calculation are as same as those in Fig. 4.

Since the space charge force prevents bunching of electrons, the FEL gain decreases and the position of saturation shifts from z/λ_w=13 to 16 as shown by the dashed curve. And the maximum value of the bunching parameter also decreases from 0.74 to 0.63.

2.4. Cubic Dispersion Relation for FELs

Using the complex rf amplitude defined by

$$\tilde{a}_s = a_s e^{i\phi}, \tag{33}$$

the KMR equations are rewritten as

$$\frac{d\gamma}{dz} = -\frac{\omega/c}{2\gamma\hat{\beta}_z} a_w f_B \, Im(\tilde{a}_s e^{i\theta}) - \hat{\varepsilon}_s \, Im\left(e^{-i\theta}\left\langle e^{i\theta}\right\rangle\right), \tag{34}$$

$$\frac{d\theta}{dz} = \Delta k + \frac{\omega/c}{2\gamma^2\hat{\beta}_z{}^3} a_w f_B \, Re\left(\tilde{a}_s e^{i\theta}\right), \tag{35}$$

$$\frac{d\tilde{a}_s}{dz} = i\frac{e\mu_0}{2mck}\frac{2I}{ab}\left\{a_w f_B\left\langle\frac{e^{-i\theta}}{\gamma\hat{\beta}_z}\right\rangle - \tilde{a}_s\left\langle\frac{1}{\gamma\hat{\beta}_z}\right\rangle\right\}, \tag{36}$$

where $\theta = \psi - \phi$, and Δk is the detuning parameter defined by

$$\Delta k = k_w + k - \frac{\omega/c}{\beta_z}. \tag{37}$$

Linearizing Eq.(34)-(36) with respect to the perturbations of $\delta\gamma/\gamma$ and $\delta\theta$ by the interaction with the electromagnetic field and picking up dominant terms with the assumption of $/\,\Gamma + \Delta k\,/ << k_w$, we obtain the approximated linearized equations of

$$\frac{dX}{dz} + i\Delta kX = i\frac{a_1}{2}\tilde{a}_s - \frac{\hat{\varepsilon}_s}{2\gamma_0}\langle Y\rangle_{\beta_z}, \tag{38}$$

$$\frac{dY}{dz} + i\Delta kY = a_2 X, \tag{39}$$

$$\frac{d\tilde{a}_s}{dz} = a_5\langle Y\rangle_{\beta_z}, \tag{40}$$

where $X = \left\langle(\delta\gamma/\gamma_0)e^{-i\theta_0}\right\rangle_{\theta_i}$, $Y = \left\langle\delta\theta e^{-i\theta_0}\right\rangle_{\theta_i}$, γ_0 and $\theta_0 = \theta_i + \Delta kz$ are unperturbed γ and θ, respectively, and a_1, a_2 and a_5 are given in Appendix B. $\langle\cdots\rangle_{\theta_i}$ and $\langle\cdots\rangle_{\beta_z}$ mean the averages on the initial values of θ and β_z, respectively. Assuming X, Y and $\tilde{a}_s$ are proportional to $e^{i\Gamma z}$ in Eqs.(38)-(40), we obtain the well known cubic dispersion relation[6,10] for Γ;

$$\Gamma^3 + 2\kappa_c\Gamma^2 + \left\{\kappa_c{}^2 - \frac{\kappa^2}{4} - A_2\right\}\Gamma + A_1 = 0, \tag{41}$$

where κ_c and κ are the center value and the spread of Δk, respectively. The coupling term A_1 between the electron beam and the electromagnetic field and the space charge term A_2 are given by

$$\kappa_c = k_w + k - \frac{\omega/c}{\hat{\beta}_z}\left(1 + \frac{a_w{}^2 k_w{}^2}{8\gamma_0{}^2\hat{\beta}_z{}^2} y_b{}^2\right), \tag{42}$$

$$\kappa = \frac{\omega/c}{\gamma_0{}^2\hat{\beta}_z{}^3}\left\{\left(1 + \frac{a_w{}^2}{2}\right)\frac{\Delta\gamma}{\gamma_0} + \frac{a_w{}^2 k_w{}^2}{4} y_b{}^2\right\}, \tag{43}$$

$$A_1 = \frac{\pi}{2k}\frac{I/I_A}{ab/2}\frac{(\omega/c)^2}{\gamma_0{}^5\hat{\beta}_z{}^5}\left(1 + \frac{a_w{}^2}{2}\right) f_B{}^2 a_w{}^2, \tag{44}$$

$$A_2 = \frac{4\pi}{k_w + k}\frac{I/I_A}{\sigma_b}\frac{\omega/c}{\gamma_0{}^3\hat{\beta}_z{}^3}\frac{\beta}{\hat{\beta}_z}\left(1 + \frac{a_w{}^2}{2}\right) J_0(\xi) f_{2D}. \tag{45}$$

For the case that the initial bunching and energy modulation are zero, i.e. $X(0) = 0$ and $Y(0) = 0$, the electromagnetic field with the initial amplitude of $\tilde{a}_s(0)$ is given by

$$\tilde{a}_s(z) = \tilde{a}_s(0)\left[\frac{\lambda_2\lambda_3 e^{i\lambda_1 z}}{(\lambda_1 - \lambda_2)(\lambda_1 - \lambda_3)} + \frac{\lambda_3\lambda_1 e^{i\lambda_2 z}}{(\lambda_2 - \lambda_3)(\lambda_2 - \lambda_1)} + \frac{\lambda_1\lambda_2 e^{i\lambda_3 z}}{(\lambda_3 - \lambda_1)(\lambda_3 - \lambda_2)}\right], \tag{46}$$

where λ_1, λ_2, and λ_3 are three roots of the dispersion relation (see Appendix B). It should be noted that since the effect of the space charge term A_2 on the electromagnetic field amplification is similar to the effect of the axial velocity spread κ, it is difficult to separate these effects in the experimental data.

To see the basic properties of the dispersion relation, we consider the case of the cold beam here. Neglecting the space charge term ($\hat{\varepsilon}_s = 0$) and assuming $\kappa = 0$ i.e. $(\Delta\gamma/\gamma)_{eff} = 0$, Eq.(41) becomes to be

$$\Gamma(\Gamma + \kappa_0)^2 = -A_1, \tag{47}$$

where $\kappa_0 = k_w + k - \omega/c\hat{\beta}_z$ is the detuning parameter for the cold beam. The maximum growth rate of $\tilde{a}_s$ is given by $[-Im(\Gamma)]_{max} = \sqrt{3}k_w\rho$ at $\kappa_0 = 0$ where ρ is so called the FEL Pierce parameter or the FEL gain parameter given by

$$\rho = \frac{A_1^{1/3}}{2k_w} \cong \frac{\pi^{1/3}}{2\gamma_0}\left(\frac{I/I_A}{ab/2}\right)^{1/3}\left(\frac{f_B a_w}{k_w}\right)^{2/3}. \tag{48}$$

The Pierce parameter gives the conversion efficiency of the beam power to the rf-power in the constant wiggler i.e. the saturation efficiency, $P_{rf}^{(sat)} \approx \rho P_b$.[9,10] For example the expected efficiency for the FEL amplifiers of LLNL and KEK are listed in Table 1.

Table1. The Pierce parameter and expected rf-power at saturation in the constant wiggler for the FEL experiments of LLNL and KEK.

	$T(MeV)$	$I(A)$	$f(GHz)$	$\rho(\%)$	$P_{sat}(MW)$
LLNL	3.0	850	34.6	6	150
KEK	1.5	600	9.4	9	80
KEK	0.8	600	9.4	8	30

To avoide gain degradation by the axial velocity spread, the effective energy spread is required to be $(\Delta\gamma/\gamma)_{eff} << \rho$. The amplified power $P_{rf}(z) \propto |\tilde{a}_s|^2$ is expressed by

$$P_{rf}(z) = \frac{1}{9}\frac{m^2c^2\omega ab}{4e^2\mu_0}\left|\tilde{a}_s(0)\left\{e^{-2i\rho k_w z} + 2e^{i\rho k_w z}\cosh\left(\sqrt{3}\rho k_w z\right)\right\}\right|^2$$
$$\approx \frac{P_{rf}(0)}{9}e^{2\sqrt{3}\rho k_w z}. \quad (\text{for } \rho k_w z >> 1) \tag{49}$$

Growth curves of the rf-power given by Eq.(46) and Eq.(49) are depicted in Fig. 9 for the cold beam ($\kappa = 0$). If the space charge effect is negligibly small, extrapolation of the growth curve $P_{rf}(z)$ in the exponential growth region to $z = 0$ gives a simple estimation of the effective input rf-power to the FEL amplifier.[6] On the other hand, if the space charge effect and/or the effective energy spread are not negligibly small, this extrapolation does not give a simple estimation of the input power as shown in this figure.

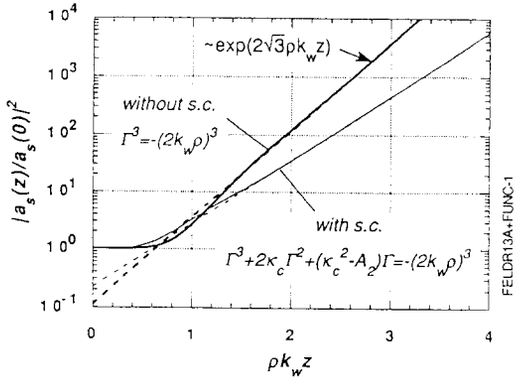

Fig. 9 Maximum growth of the rf-power predicted by the cold beam (κ=0) dispersion relation. The solid line and the thin line are the calculated growth curves without and with the space charge effect, respectively.

To show the resonance shift and gain degradation by the space charge effect, the exponential gain as a function of the wiggler field, so called detuning curve, calculated from the dispersion relation of Eq.(41) is shown in Fig. 10. The parameters of the FEL are chosen to be close to the LLNL FEL amplifier[22] except for the single mode approximation. If we ignore the space charge effect, the peak gain of 36dB/m is expected at B_w=3.55kG where the peak gain is restricted by the axial velocity spread of electrons due to the finite beam size. If the space charge effect is taken into account in the calculation, the peak gain decreases to 26dB/m and the peak position shifts toward low B_w side by 150G for the space charge reduction factor f_{2D} given by Eq.(30). If we assume the reduction factor given by Eq.(A13) in Appendix A, we have smaller shift and gain degradation than this example as shown in Fig. 10. It may be difficult to make clear this difference because of other ambiguities of the experimental parameters.

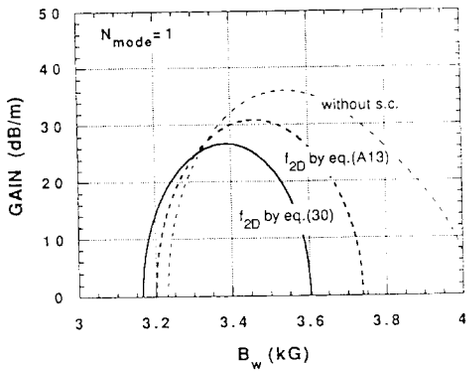

Fig. 10 The FEL gain taking account of κ_c and κ as a function of the wiggler field. The solid line is the gain curve without the space charge effect. The dashed line and the thin dashed line are gain curves for the space charge reduction factors given by Eq. (30) and Eq. (A13), respectively. The parameters for the calculation are T=3MeV, I=850A, λ_w=9.8cm, f=34.6GHz, $a\times b$=10cm×3cm, N_{mode}=1 and $r_b = y_b$ =5mm.

3. Experiments on High Power FELs in the Microwave Regime

Numerous experimental programs on high power FEL amplifiers in the microwave regime have been established and are also in progress at many laboratories and universities, LLNL, NRL, MIT, JINR, JAERI, KEK, CESTA, etc. In 1991 M.E.Conde et al. demonstrated efficiency enhancement to 27% of the FEL amplifier employing the untapered helical wiggler with reversed guide field and obtained 61MW amplified rf power at 33GHz.[19] Although their investigation is quite interesting for the FEL physics, we will discuss other 3 typical FEL experiments related to the application for accelerators in the following because of lack of the space.

3.1. The 35GHz FEL Amplifier at LLNL

Excellent experimental studies on the high power FEL amplifier in the microwave regime were carried out at the Electron-Laser Facility (ELF) of LLNL in 1980's.[4,5,6] The high current electron beam was generated by the 3.5MeV induction linac (ETA). The

electron beam of 850A with the normalized brightness of 2×10^4A/(cm·rad)^2 passed through the emittance selector was injected to the interaction region in the oversized waveguide with the cross section of 10cm×3cm as shown in Fig. 11.[20] The wiggler was a 3m long planar wiggler consisting of reversed solenoid pairs with the period length of λ_w=9.8cm.

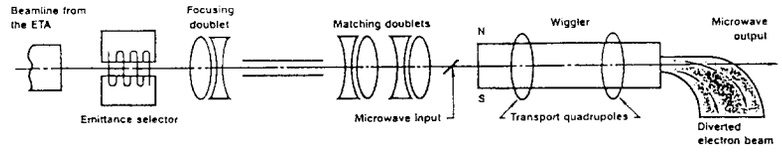

Fig. 11 The 35GHz FEL amplifier at LLNL (ref. 20).

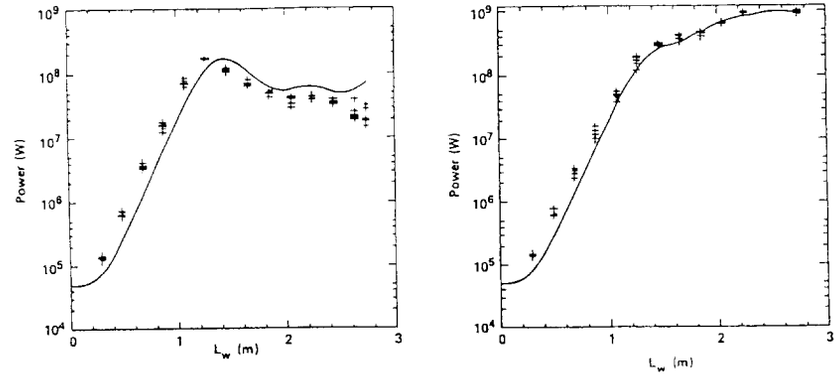

Fig. 12 Amplified rf-power in the FEL for the constant wiggler (a) and for the tapered wiggler (b) of the LLNL FEL amplifier (ref. 5).

They demonstrated saturation of the FEL with a saturated power of 180MW (η=6%) and the efficiency enhancement to η=34% with the 1GW amplified rf-power by tapering the wiggler field at 34.6GHz as shown in Figs. 12(a) and (b). The measured exponential gain was 34dB/m which is reproduced by the 2D simulation code FRED. Since the difference of

the resonance energy between the $TE_{21}(TM_{21})$ and TE_{01} modes is only ~2.6%, comparable power of the fundermental mode was measured in the higher-order mode (Fig 13).[21] The measured results were consistent to analysises including higher-order mode by the dispersion relation and the simulation code FRED except for the rf-phase evolution beyond saturation in the constant wiggler.[4,21,22,23]

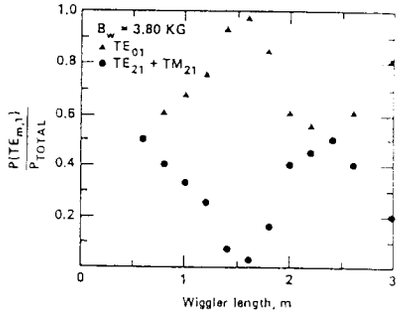

Fig. 13 Measured fraction of total rf-power in the TE_{01} mode and in the TE_{21} and TM_{21} modes (ref. 21)

3.2. The Ion-Channel Guided X-band FEL Amplifier at KEK

To investigate the feasibility of the FEL as an rf-power source for the linear collider, the X-band microwave FEL has been studied experimentaly at KEK.[24,25,26,27] In the concept of a TBA/FEL, a high current electron beam for driving FELs passes through many stages of FELs and induction units for reaccelerating the beam, and we will meet the difficulty of beam transportation due to the strong BBU. To suppress the BBU in the induction linac ATA at LLNL, the ion-channel guiding was demonstrated successfully to transport the 7kA electron beam.[28] This experiment suggests the efficacy of the nonlinear focusing field in the ion-channel to suppress the BBU in a TBA/FEL. To investigate the focusing performance for the FEL drive beam, the ion focusing FEL amplifier at 9.4GHz has been studied at KEK. The electron beam was generated by the 0.8-1.6MeV induction linac and guided by the ion-channel formed by irradiation of the KrF laser of ~140mJ in the diethylaniline (DEA) gas filled in the beam path at 0.5-1 mtorr as shown in Fig. 14. The electron beam of 500-600A passed through the emittance selector was injected into the wiggler region. The wiggler was a planar wiggler with 15 periods and a period length of

λ_w=16cm. The 9.4GHz rf-power of 77kW was fed through the input coupler with ~90% transmission efficiency to the interaction region in the oversized waveguide with the cross section of 11cm×5.5cm. It is expected that the higher order mode exitation in the FEL interaction should be small because the resonance energy of the TE_{21} mode differs from that of the TE_{01} mode by 15%. At 1.5MeV operation, maximum performance of beam transportation in the wiggler and of the rf amplification was obtained with the ion density of 2×10^{10} cm^3.

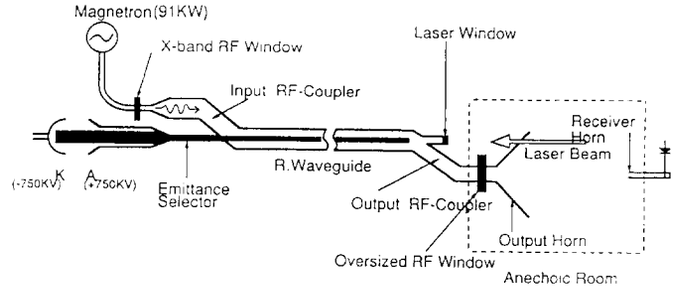

Fig. 14 The ion-channel guided FEL amplifier at KEK.

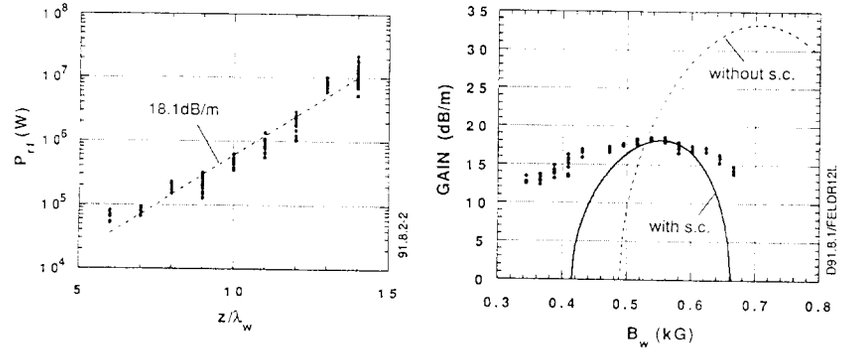

(a) (b)

Fig. 15 (a) Amplified rf power as a function of z/λ_w at 0.8MeV operation. (b) Exponential gain as a function of B_w where the solid line and the dashed line are calculations with and without the space charge effect, respectively, for T=0.78MeV, I=650A and $(\Delta\gamma/\gamma)_{eff}$=2.4% ($\Delta\gamma/\gamma_0$ =0 and $r_b = y_b$ =15mm).

In the FEL amplifier operated at 800keV, the maximum gain of 18-19dB/m and the amplified rf power of ~30MW were measured as shown in Figs. 15(a) and (b). In this operation the FEL gain was limited by the space charge effect. At the beam energy of 1.48MeV, the exponential gain of 20-21dB/m was obtained at B_w=1.21kG and the FEL amplifier saturated at z/λ_w=12 with the saturation power of 100MW as shown in Figs. 16(a) and (b). Power growth in the wiggler is well reproduced by the 1D simulation with $(\Delta\gamma/\gamma)_{eff}$=5.6% ($\Delta\gamma/\gamma$=0 and $r_b = y_b$ =15mm). In the calculation of the detuning curve, $(\Delta\gamma/\gamma)_{eff}$=7.8% ($\Delta\gamma/\gamma$=0 and $r_b = y_b$ =18mm) is assumed to fit the maximum gain. The fraction of the total rf power in the higher order modes was less than a few percents as expected. These results mean that the FEL performance at 1.5MeV operation is limited by the beam emittance and not space charge, and the availability of the ion-focused elctron beam for the single stage FEL amplifier is also demonstrated. After this experiment, the experimental study on the FEL amplifier driven by a bunched electron beam is in progress at KEK to investigate the basic properties of the interstage FEL in the multistage FEL in a TBA/FEL concept.[29]

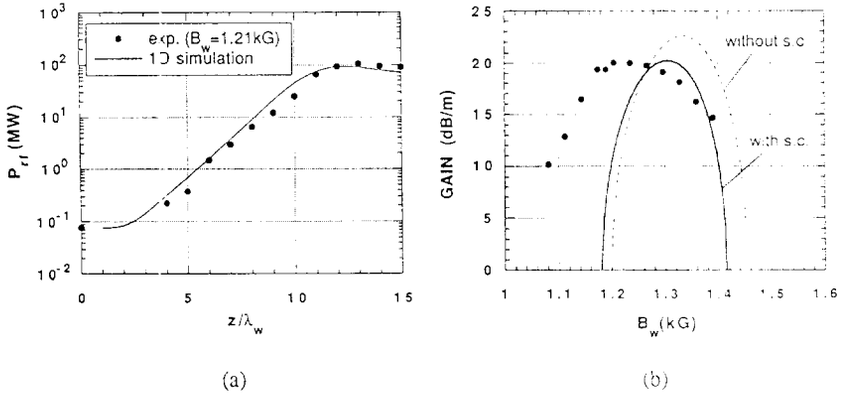

Fig. 16 (a) Amplified rf power in the KEK FEL at the beam energy of 1.48MeV as a fuction of z/λ_w. The curve is the 1D simulation with I = 600A and B_w = 1.26kG. (b) The exponential gain as a function of B_w. The solid curve and the dashed curve are the calculated gain by the dispersion relation with and without the space charge effect, respectively, for I = 600A.

3.3. Beam Buncher for the CLIC Driving Beam .

In the CLIC project at CERN[30], the accelerating rf for the main linac will be generated by the rf transfer structure which is the resonant structure driven by a high current bunch train of electrons with the frequency of 30GHz as shown in Fig. 17. They have an optional plan to generate the driving beam for the rf transfer structure using an induction linac and a microwave FEL (FEM).[14,31] As shown in Fig. 18, the bunching parameter of 80% is expected for the FEL with a helical wiggler which is driven by a electron beam of 4kA and 9.5MeV[15]. The expected bunching performance of the FEL is shown in Fig. 19 where very sharp electron bunches with the peak current of I/I_0 ≈9-9.5 are expected at 30GHz for the average beam current of I_0. The experimental investigation on the bunching performance of the FEL is in progress at CESTA[16].

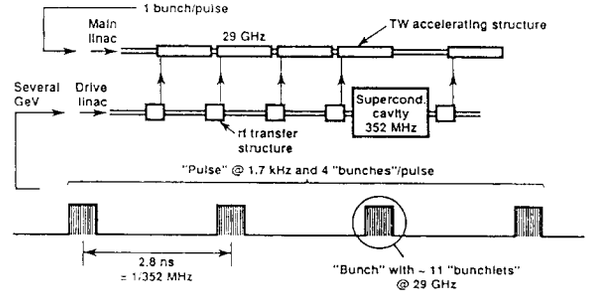

Fig. 17 The CLIC-TBA concept. The high energy beam in the main linac is accelerated to 1TeV . The accelerating rf is generated in the rf-transfer structure driven by a bunched electron beam at 29-30 GHz with the energy of 3 GeV (ref. 14).

The FEL amplifier with a helical wiggler driven by the 1.75MeV pulse line accelerator produced the saturation power of 50MW at 35GHz, and the coherent radiation from the beam passed through the FEL interaction region was observed. Next program of the FEL driven by a 2.5MeV induction linac with the beam current of 1kA is going on at CESTA where the banching parameter of ~40% is expected.

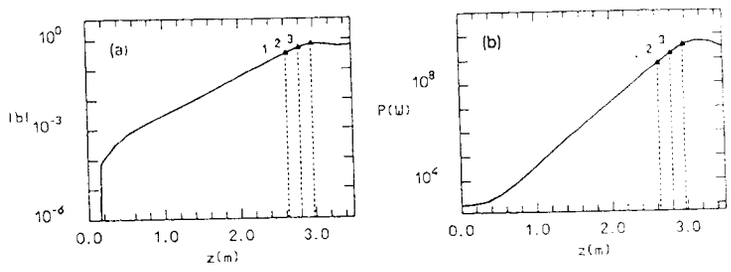

Fig. 18 (a) The expected bunching parameter and (b) the amplified rf power in the 30 GHz FEL driven by an induction linac with I=4kA at 9.5 MeV (ref. 15).

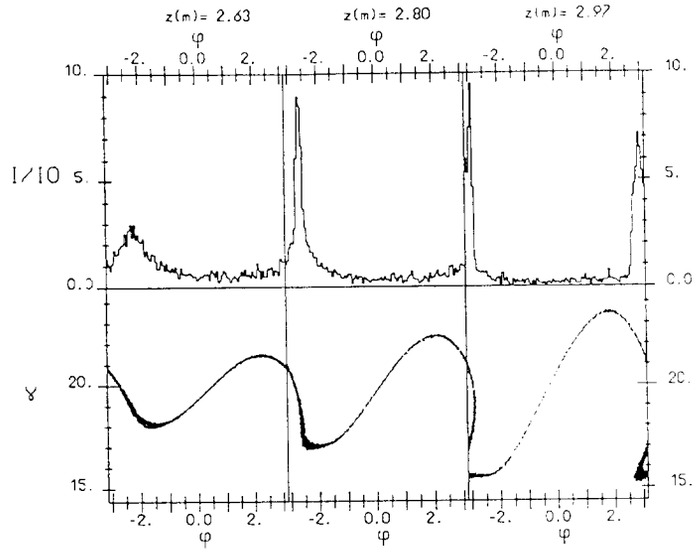

Fig. 19 (a) The instanteneous electron current in a period of y and (top) and the electron distribution in the (ψ,γ) phase space (bottom) of the FEL (ref. 15).

4. Appendices

4.1. Appendix A: Longitudinal Space Charge Field

To calculate the space charge field taking account of the wiggle motion of the electron beam, the s-component of the Maxwell equation given by Eq.(28) is solved in an approximated manner. We assume that the electron orbit is determined by the planar wiggler field alone and the wiggler field is approximated by $\boldsymbol{B}_w = B_w \cos k_w z \cdot \boldsymbol{e}_y$. We define the (u,v,s) system by the Frenet-Sere orthonormal unit vectors of $\boldsymbol{e}_s = \beta_0/\beta$, $\boldsymbol{e}_u = \boldsymbol{e}_y \times \beta_0/\beta$ and $\boldsymbol{e}_v = \boldsymbol{e}_y$ as shown in Fig. 7 where $c\beta_0$ is the electron velocity at the beam center, $\boldsymbol{e}_s$ is the instantaneous direction of the wiggle motion and s is the length along the beam center orbit. From the periodicity of the ponderomotive force the beam charge density and the space charge field may be expanded as

$$\rho = N(u,v) \sum_{n=-\infty}^{\infty} \rho_n e^{in\theta}, \tag{A1}$$

$$E_s = \sum_n \varepsilon_n(u,v) e^{in\theta}, \tag{A2}$$

$$E_u = \sum_n \eta_n(u,v) e^{in\theta}, \tag{A3}$$

where $\theta(u,v) = (k_w + k)z(u,v) - \omega t$, $N(u,v)$ is the beam profile function, $E_s = \boldsymbol{E}_{sp} \cdot \boldsymbol{e}_s$ and $E_u = \boldsymbol{E}_{sp} \cdot \boldsymbol{e}_u$. The explict expression of Eq.(28) is written by

$$\frac{\partial^2 E_s}{\partial u^2} - \frac{\kappa}{1-u\kappa}\frac{\partial E_s}{\partial u} + \frac{\partial^2 E_s}{\partial v^2} + \frac{1}{(1-u\kappa)^2}\frac{\partial^2 E_s}{\partial s^2} + \frac{u\kappa'}{(1-u\kappa)^3}\frac{\partial E_s}{\partial s} - \frac{\kappa^2}{(1-u\kappa)^2}E_s - \frac{1}{c^2}\frac{\partial^2 E_s}{\partial t^2}$$
$$- \frac{2\kappa}{(1-u\kappa)^2}\frac{\partial E_u}{\partial s} - \frac{\kappa'}{(1-u\kappa)^3}E_u$$
$$= \frac{1}{\varepsilon_0}\frac{1}{1-u\kappa}\frac{\partial \rho}{\partial s} + \mu_0 \frac{\partial J_s}{\partial t}, \tag{A4}$$

where $J_s = c\beta_s \rho$ and κ is the instantaneous curveture of the beam center orbit;

$$\kappa = \frac{1}{\beta_{0z}}\frac{d\beta_{0x}(s)}{ds}. \tag{A5}$$

To solve Eq.(A4) in the lowest order approximation, we neglect the s-dependence of ε_n, η_n and N, and assume the round beam with the radius of r_b. Changing the variables from (u,v) to (r,ϕ) defined by $u = r\cos\phi$ and $v = r\sin\phi$ and averaging Eq.(A4) in the interval of $s_w = \lambda_w\beta/\hat{\beta}_z$ which is the length of s corresponding to a wiggler period, we obtain the equation for ε_n in the lowest order approximation where ε_n does not depend on ϕ and small quantities in the order of $O\left(a_w^4/4\gamma^4\hat{\beta}_z^4\right)$ are ignored;

$$\frac{d^2\varepsilon_n}{dr^2}+\left(1-\frac{r^2}{2}\left\langle k^2\right\rangle_s\right)\frac{1}{r}\frac{d\varepsilon_n}{dr}-\left[n^2\left\{(k_w+k)^2-\frac{\omega^2}{c^2}\right\}+\left\langle\kappa^2\right\rangle_s\right]\varepsilon_n$$
$$=i\frac{\rho_n}{\varepsilon_0}\frac{\langle\beta_{0z}\rangle_s}{\beta}n\left\{(k_w+k)-\frac{\omega\beta}{c\hat{\beta}_z}\right\}N(r), \tag{A6}$$

where $\langle\cdots\rangle_s$ means the average on s in the interval of s_w and the terms depending on η_n vanish by averaging on ϕ. In the region of $r^2\left\langle\kappa^2\right\rangle_s << 1$, Eq.(A6) is approximated to be

$$\frac{d^2\varepsilon_n}{dr^2}+\frac{1}{r}\frac{d\varepsilon_n}{dr}-n^2g^2\varepsilon_n=i\frac{nh\rho_n}{\varepsilon_0}N(r), \tag{A7}$$

where

$$g^2=(k_w+k)^2-\frac{\omega^2}{c^2}+\frac{k_w^2}{n^2}\left(1-\frac{\hat{\beta}_z^2}{\beta^2}\right)\approx\frac{(k_w+k)^2}{\gamma_z^2}, \tag{A8}$$

$$h=\frac{k_w+k}{\beta}\hat{\beta}_z-\frac{\omega\beta}{c}\approx\frac{k_w+k}{\gamma^2}\frac{\hat{\beta}_z}{\beta}, \tag{A9}$$

and $\gamma_z = 1/\sqrt{1-\hat{\beta}_z^2}$. Assuming the boundary condition of $\varepsilon_n = 0$ at $r = b/2$ and the uniform charge distribution in the beam cross section, i.e. $N(r) = 1$ for $r < r_b$, we have

$$\varepsilon_n(r)=-i\frac{\rho_n h}{\varepsilon_0 ng^2}\left\{1-ngr_bf_nI_0(ngr)\right\}, \tag{A10}$$

where

$$f_n=\frac{I_0(ngb/2)K_1(ngr_b)-K_0(ngb/2)I_1(ngr_b)}{I_0(ngb/2)}=K_1(ngr_b). \tag{A11}$$

For $n(k_w+k)r/\gamma << 1$, $\varepsilon_n(r)$ is approximated to be

$$\varepsilon_n(r)\approx -i\frac{\rho_n}{n\varepsilon_0(k_w+k)}f_{2D}, \tag{A12}$$

where f_{2D} is the space charge reduction factor due to the finite beam size;

$$f_{2D}=\frac{\gamma_z^2\hat{\beta}_z}{\gamma^2\beta}\left[1-\frac{n(k_w+k)}{\gamma_z}r_bK_1\left\{\frac{n(k_w+k)}{\gamma_z}r_b\right\}\right]. \tag{A13}$$

On the other hand, E.T.Scharlemann et al.[22] gave the expression of the reduction factor of

$$f_{2D}=1-\frac{n(k_w+k)}{\gamma}r_bK_1\left\{\frac{n(k_w+k)}{\gamma}r_b\right\}, \tag{A14}$$

which has different γ dependence from Eq.(A13). This reduction factor is obtained by ignoring the terms introduced by $\partial\theta/\partial u=-(k_w+k)\beta_{0x}/\beta$ in the 1st term of Eq.(A4). The ratio of these reduction factors is

$$f_{2D}(Eq.(A13))/f_{2D}(Eq.(A14))\approx\gamma_z/\gamma<1,$$

therefore f_{2D} of Eq.(A13) gives smaller space charge field than that given by Eq.(A14). For example, in the LLNL 35GHz FEL experiment, the ratio of reduction factors is $\gamma_z/\gamma = 2.7/6.9 = 0.4$. In the limit of $kr_b >> 1$, we have the limits of $f_{2D}(Eq.(A14))\to 1$ and $f_{2D}(Eq.(A13))\to\gamma_z^2/\gamma^2$ where γ_z^2/γ^2 represents the reduction of the longitudinal space charge field E_s by the wiggle motion. The remarkable difference between these results is the energy dependence of the space charge field. In Eq.(A13) the space charge field decreases in proportional to γ^{-2}, however, γ^{-1} in Eq.(A14). This difference may be important for the consideration on the optimum energy of the driving beam in the TBA/FEL concept.

4.2. *Appendix B: Cubic Dispersion Relation*

Following to ref.(6) and ref.(10), the cubic dispersion relation for an FEL and the expression of amplitude growth of the amplified electromagnetic field are derived by linearizing KMR equations. Let $\delta\gamma = \gamma - \gamma_0$ and $\delta\theta = \theta - \theta_0$ be the perturbations by the interaction with the radiation field where γ_0 and $\theta_0 = \theta_i + \Delta kz$ are the unperturbed γ and θ, respectively, and θ_i is the initial θ_0. Linearizing Eqs.(34)-(36) with respect to $\delta\gamma/\gamma$ and $\delta\theta$, we have

$$\frac{dX}{dz} + i\Delta kX = i\frac{a_1}{2}\tilde{a}_s - \frac{\hat{\varepsilon}_s}{2\gamma_0}\langle Y\rangle_{\beta_z}, \tag{B1}$$

$$\frac{dY}{dz} + i\Delta kY = a_2 X + \frac{a_3}{2}\tilde{a}_s, \tag{B2}$$

$$\frac{d\tilde{a}_s}{dz} = -ia_4\langle X\rangle_{\beta_z} + a_5\langle Y\rangle_{\beta_z} - ia_6\tilde{a}_s, \tag{B3}$$

where $X = \left\langle (\delta\gamma/\gamma_0)e^{-i\theta_0}\right\rangle_{\theta_i}$, $Y = \left\langle \delta\theta e^{-i\theta_0}\right\rangle_{\theta_i}$ and

$$a_1 = \frac{\beta_{z0}^2}{2}\frac{f_B a_w}{1 + a_w^2/2}\, a_2 = \beta_{z0}^2 a_3 = \frac{\omega/c}{2\gamma_0^2\beta_{z0}} f_B a_w, \tag{B4}$$

$$a_4 = \frac{a_5}{\beta_{z0}^2} = \frac{f_B a_w}{\beta_{z0}^2}\, a_6 = \frac{2\pi}{k}\frac{I/I_A}{ab/2}\frac{f_B a_w}{\gamma_0\beta_{z0}^3}. \tag{B5}$$

Since the last terms in the right hand sides of Eqs.(B2) and (B3) have small contributions and $a_4 X/a_5 Y \approx (\Gamma + \Delta k_0)/k_w$, the terms proportional to a_3, a_4 and a_6 can be ignored by assuming $|\Gamma + \Delta k_0| << k_w$ and we obtain the approximated linearized equations of Eqs.(38)-(40). Substituting $\tilde{a}_s = a_s e^{i\Gamma z}$ into Eqs.(38)-(40), we have the cubic dispersion relation for Γ;

$$\Gamma^3 + 2\kappa_c\Gamma^2 + \left\{\kappa_c^2 - \frac{\kappa^2}{4} - A_2\right\}\Gamma + A_1 = 0, \tag{B6}$$

where $A_1 = a_1 a_2 a_5/2$ and $A_2 = \hat{\varepsilon}_s/2\gamma_0$. Using the roots $(\lambda_1, \lambda_2, \lambda_3)$ of the dispersion relation of Eq.(B6), the solution of $\tilde{a}_s$ is written by

$$\tilde{a}_s(z) = \xi_1 e^{i\lambda_1 z} + \xi_2 e^{i\lambda_2 z} + \xi_3 e^{i\lambda_3 z}. \tag{B7}$$

The coefficients ξ_1, ξ_2 and ξ_3 are determined by the initial condition. For the case of $X(0) = 0$ and $Y(0) = 0$, i.e., zero initial bunching and energy modulation, the initial condition given by Eqs.(38)-(40) is written by

$$\xi_1 + \xi_2 + \xi_3 = \tilde{a}_s(0), \tag{B8}$$

$$\lambda_1\xi_1 + \lambda_2\xi_2 + \lambda_3\xi_3 = 0, \tag{B9}$$

$$\lambda_1^2\xi_1 + \lambda_2^2\xi_2 + \lambda_3^2\xi_3 = 0, \tag{B10}$$

and we obtain the explicit expression Eq.(46) for $\tilde{a}_s(z)$, which is a bit different from $\tilde{a}_s(z)$ given in ref.(10) because the approximated equations of Eqs.(38)-(40) are slightly different from those in ref.(10).

5. References

1. R.M.Phillips, Nucl. Instr. and Meth. A272(1988)1.
2. L.R.Elias et al., Phys. Rev. Lett. 36(1976)717.
3. D.A.G.Deacon et al., Phys. Rev. Lett. 38(1977)892.
4. T.J.Orzechowski et al., IEEE J. Quantum Electr. QE-21(1985)831.
5. T.J.Orzechowski et al., Phys. Rev. Lett. 57(1986)2127.
6. T.J.Orzechowski et al., Phys. Rev. A35(1987)2184.
7. A.M.Sessler, AIP Cof. Proc., 91(1982)154.
8. A.M.Sessler et al., Nucl. Instr. and Meth. B40/41(1989)1064.
9. C.W.Roberson and P.Sprangle, Phys. Fluids B1(1989)3.
10. J.B.Murphy and C.Pellegrini, Laser Handbook, vol.6, ed. W.B.Colson et al., (North-Holland, Amsterdam, 1990), p.9.
11. E.T.Scharlemann, J. Appl. Phys. 58(1985)2154.
12. N.M.Kroll et al., IEEE J. of Quantum Electronics QE-17(1981)1436.
13. E.T.Scharlemann, Laser Handbook, vol.6, ed. W.B.Colson et al., (North-Holland, Amsterdam, 1990), p.291.
14. H.D.Shay et al., Nucl. Instr. and Meth. A304(1991)262.
15. W.A.Barletta et al., Nucl. Instr. and Meth. A329(1993)348.
16. J.Gardelle et al., Proc. 16th Int. FEL Conf., Stanford Univ., 1994; to be published in

Nucl. Instr. and Meth. A.
17. D.B.Hopkins et al., LBL-25936, LBL, 1988.
18. R.A.Jong et al., Nucl. Instr. and Meth. A296(1990)776.
19. M.E.Conde and G.Bekefi, Phys. Rev. Lett. 67(1991)3082.
20. Energy and Technology Review, LLNL, 1986.
21. T.J.Orzechowski et al., Nucl. Instr. and Meth. A250(1986)144.
22. E.T.Scharlemann et al., Nucl. Instr. and Meth. A250(1986)150.
23. J.Wurtele et al., Nucl. Instr. and Meth. A250(1986)176.
24. S.Hiramatsu et al., Part. Accelerators 31(1990)75.
25. T.Ozaki et al., Nucl. Instr. and Meth. A318(1992)101.
26. D.H.Whittum et al., IEEE Trans. on Plasma Sci. 21(1993)136.
27. K.Takayama et al., to be published in Appl. Phys. Lett. (KEK Preprint 94-182, KEK, 1994).
28. G.J.Caporaso et al., Phys. Rev. Lett. 54(1986)1591.
29. S.Hiramatsu, Proc. Workshop on Pulsed RF Power Sources for Linear Colliders, Dubna-Protvino, 1993, p.293.
30. W.Schnell, Proc. Workshop on Physics of Linear Colliders, Capri, 1988, p.345.
31. C.D.Johnson, Proc. 17th Int. Linac Conf., Tsukuba, Aug. 21-26, 1994; to be published.